processes

MDPI

Article

Mechanisms of Groundwater Damage to Overlying Rock in Goaf

Nan Zhu [1,2], Fei Liu [3,*] and Dafa Sun [2]

[1] School of Environment and Spatial Informatics, China University of Mining and Technology, Xuzhou 221116, China; zhunan@ahszu.edu.cn
[2] School of Environment and Surveying Engineering, Suzhou University, Suzhou 234000, China
[3] School of Resources and Civil Engineering, Suzhou University, Suzhou 234000, China
* Correspondence: szxylf@126.com

Abstract: The discontinuation of pumping and drainage activities upon the cessation of mining operations leads to the gradual accumulation of groundwater. This inflow into mined-out areas affects the properties of the rock, disturbing the previously stable goaf and exacerbating instability. In this study, we advance an existing theoretical framework pertaining to the residual deformation of mines by delineating the mechanisms through which groundwater influences the degradation of the overlying strata in goaf areas. Using analogous material simulation experiments and rigorous theoretical analyses, we clarify the specific mechanisms by which groundwater causes structural damage to these regions. The deformation of overlying rock is divided into three different forms: the compressive deformation of rock, the sliding instability of rock, and the rotational instability of rock. The main contributions of this study are its refinement of the existing theory of the residual deformation of mines, an analysis of the damage mechanisms of groundwater, and suggestions regarding technical support for targeted treatment measures in affected mines.

Keywords: gob area; groundwater; overburden damage; formation mechanism

Citation: Zhu, N.; Liu, F.; Sun, D. Mechanisms of Groundwater Damage to Overlying Rock in Goaf. *Processes* **2024**, *12*, 936. https://doi.org/10.3390/pr12050936

Academic Editor: Blaž Likozar

Received: 8 April 2024
Revised: 30 April 2024
Accepted: 1 May 2024
Published: 4 May 2024

1. Introduction

Coal has always been a fundamental raw energy material in China. Data from the annual *China Statistical Yearbook*, *Coal Industry Development Annual Report*, and *China Mineral Resources Report* indicate that the output of raw coal has continuously increased since its nadir in 2016, and there is a rising trend in the growth rate. China's annual coal output in 2022 was 4.56 billion tons, and coal accounted for approximately 67% of China's primary energy in 2021. The share of coal resources has declined with adjustments to China's energy structure, but coal still plays a dominant role. It is likely that coal will remain the main energy source for a long time.

Coal resources in certain areas have gradually been depleted because of long-term mining. Mining conditions have become more complex, the cost has increased, and the number of coal mines in China has decreased year by year. There were 7688 mines in 2016 but fewer than 4400 in 2022, a drop of 42.8% in five years. The main method of coal resource mining in China is underground mining, which forms many goaf areas after coal-seam mining [1,2]. The total area of coal-mining subsidence in China has reached 20,000 km^2. This is distributed over 151 counties (cities and districts) in 23 provinces (cities and districts) [3,4]. Using a calculation based on 3.8 billion tons, the resultant new subsidence area equates to 329 million hectares per year [5]. Pumping and drainage cease when mines close, and groundwater gradually accumulates. These closed coal mines accumulate water in their goaves [6]. Once the surface movement and deformation of a goaf site reach a basically stable state, the site becomes an unstable site (or an unstable site becomes more unstable) under the action of these factors because of the influence of groundwater [7,8]. Water accumulation in an old goaf not only endangers the production of surrounding mines but also "reactivates" the broken rock mass in the goaf that was

originally in a relatively balanced state. This reactivates the overlying rock layer of the goaf, resulting in further surface movement and deformation, thus destabilizing the surface site. There is no adjacent mining area around a general old goaf. The main factors causing site activation are external forces such as groundwater erosion and external loads.

Extensive research has been conducted on the impact of groundwater on goaves, and various research results have been published [9–16]. Researchers have performed comprehensive experiments on rock compaction under various conditions and have studied rock seepage in different circumstances. Different research methods have been combined to study the "activation" mechanisms of old goaves.

Most studies have only analyzed the impact of water on rock; few have examined the impact of water on goaf activation. Questions remain, such as "what are the effects of water on goaf rock layers?" And "what is the formation mechanism?" Understanding the influencing mechanisms is of significance when formulating effective mitigation measures and for disaster prevention and control. There are limited studies on the formation mechanisms of this type of damage at present. Our main research objective was to conduct an in-depth study of the formation mechanisms of this phenomenon using model tests with similar materials based on a theoretical analysis. The purposes of our study were to improve the existing theory of the residual deformation of mines and to provide technical support for relevant mines to implement targeted treatment measures.

2. An Overview of the Study Area and Experimental Program

The study area was located in Huainan City, Anhui Province. It comprised an old goaf which was primarily formed from the 1960s to the 1990s, indicating its considerable age. The mining depths ranged from approximately 210 to 410 m. The coal-bearing strata belonged to the Carboniferous–Permian series. The total thickness of the Upper Carboniferous Taiyuan Formation was approximately 120 m, and the coal seams within it averaged a total thickness of 7.80 to 9.88 m. The upper Permian strata, which included D and E coal groups, had a total thickness of 330 m. After 2000, a new and modernized coal production square was constructed to increase coal production. This was located approximately one kilometer from the old industrial square. The new industrial square was built on the stable ground of the original goaf. However, damage occurred to the buildings within the industrial square following its activation. Seventy-one monitoring points were established through the deployment of multiple observation lines that were placed on both the surface and buildings. Subsidence was detected during a long-term observation period.

A model based on the geological mining conditions and engineering foundations of the study area and using similar materials was established. The principles of the similar materials were simulated to reveal the residual deformation characteristics of the old goaf's foundation.

2.1. Model Test Bench and Related Instruments

A two-dimensional analog test platform for similar materials with a size of 2.5 m × 0.15 m was used to conduct the experiment. A DH3818 static strain acquisition system was used to record the changes in the pressure box data during mining. Rock displacement changes were observed using digital photographic measurement technology, as presented in Figure 1. The digital image analysis used a digital photographic measurement software system.

2.2. Similar Model Parameters

Our test simulated a rock layer with a total thickness of 253 m and a seam thickness of 8.0 m. Considering the purpose of this test as well as the geological and mining conditions and the size of the model frame, the size of the similar-material model was determined to be 2500 × 150 × 1265 mm. This was directly simulated to the surface. A geometric similarity ratio of Cl = 1:200 and a unit weight ratio of 0.6 (based on the characteristics of

the overlay and the simulated material) were used as similarity constants. The stress ratio and time ratio were obtained using the following formulae:

$$\alpha_\sigma = \alpha_\gamma \times \alpha_l = 0.6 \times (1/200) = 0.003, \quad (1)$$

$$\alpha_t = \sqrt{\alpha_l} = \sqrt{1/200} = 0.071, \quad (2)$$

where α_σ is the stress ratio, α_γ is the unit weight ratio, α_l is the geometric size ratio, and α_t is the time ratio.

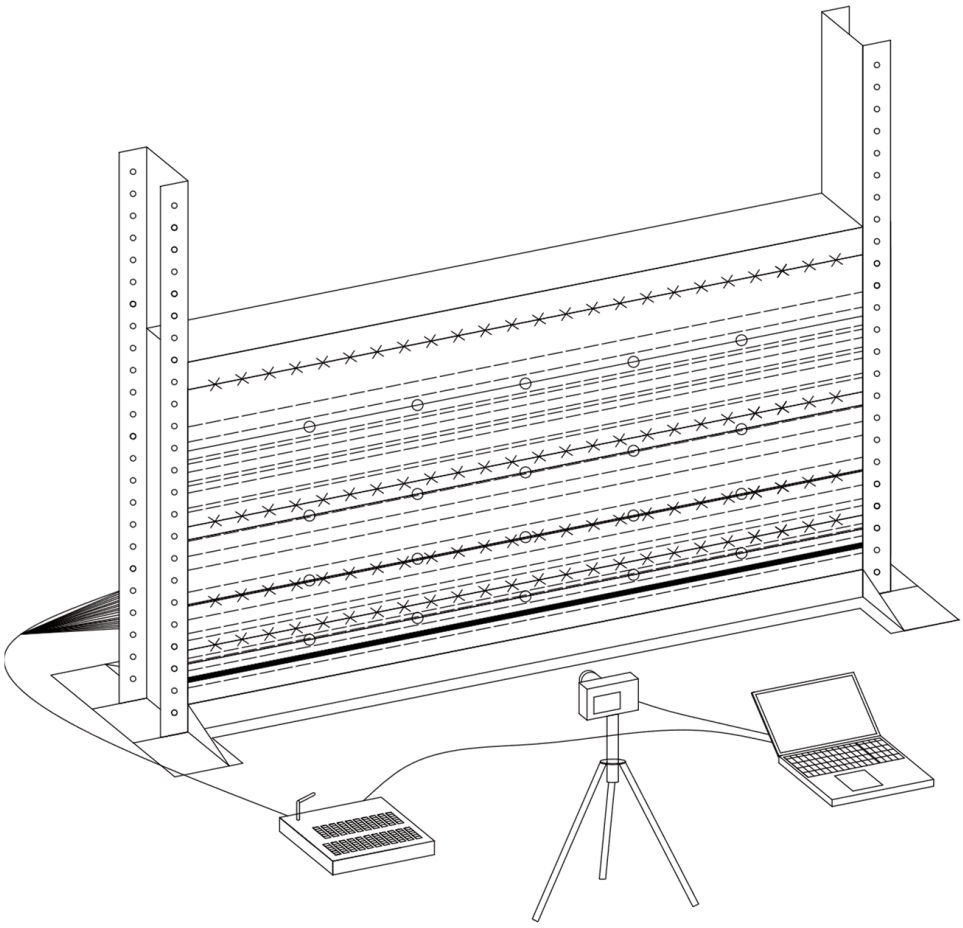

Figure 1. Two-dimensional analog test platform for similar materials.

2.3. Ratios of Similar Materials

The strength of each layer in the model test was calculated based on the original rock-strength data and a principle of similarity test. Ordinary fine river sand (containing particles with a diameter less than 3 mm) was selected as the aggregate. Gypsum and calcium carbonate were selected as the cementing materials. In accordance with the research of Luo and Yang [17,18], a reasonable proportion of samples was prepared for a strength verification test, and the ratio parameters of each layered material in this model were finally determined, as revealed in Table 1.

2.4. Measuring Point Layout

The mining direction of the simulated coal seam in the test was from left to right. Changes in the overall displacement of the model were monitored by placing pressure and displacement lines in the model.

The position of the key layer in the model was determined based on the strength and stiffness conditions of the key layer according to a drilling column diagram and a rock mechanical property table. Four observation lines were set in the model to simulate and

study the failure laws of the overlying rock. These observation lines were numbered 1, 2, 3, and 4 from top to bottom. Observation lines No. 2, No. 3, and No. 4 were located above the key layer; observation line No. 1 was a horizontal observation line arranged in the near-surface loose layer. The distance between the adjacent points of each observation line was approximately 10 cm. Figure 2 presents the arrangement of the measuring points of the model.

Table 1. Ratio parameters of layered materials.

Rock Name	Rock Thickness/m	Model Thickness/cm	Sand/kg	Calcium Carbonate/kg	Gypsum/kg	Total Mass/kg
Surface soil layer	47	23.5	126.90	4.23	9.87	141.00
Sandstone	11	5.5	28.29	1.41	3.30	33.00
Sandy mudstone	13	6.5	33.43	2.23	3.34	39.00
Gray mudstone	3	1.5	7.71	0.64	0.64	9.00
Sandy mudstone	6	3	15.43	1.03	1.54	18.00
Gritstone	7	3.5	18.90	0.63	1.47	21.00
Sandy mudstone	3	1.5	7.71	0.51	0.77	9.00
Fine sandstone	5	2.5	12.50	0.75	1.75	15.00
Sandy mudstone interbedded with sandstone	11	5.5	28.29	1.89	2.83	33.00
Sandstone	3	1.5	7.71	0.39	0.90	9.00
Mudstone interbedded with sandy shale	21	10.5	54.00	3.60	5.40	63.00
Medium-grained sandstone	11	5.5	29.33	1.10	2.57	33.00
Sandy mudstone	10	5	25.71	1.71	2.57	30.00
Sandstone	16	8	41.14	2.06	4.80	48.00
Sandy mudstone	20	10	51.43	3.43	5.14	60.00
Fine sandstone	10	5	25.00	1.50	3.50	30.00
Mudstone	5	2.5	12.86	1.07	1.07	15.00
Sandy mudstone	7	3.5	18.00	1.20	1.80	21.00
Fine sandstone	6	3	15.00	0.90	2.10	18.00
Medium-grained sandstone	3	1.5	8.00	0.30	0.70	9.00
Mudstone	6	3	15.43	1.29	1.29	18.00
Fine-grained sandstone	5	2.5	12.50	0.75	1.75	15.00
Coal	8	4	8.93	0.89	0.38	10.20
Fine-grained sandstone	4	2	10.00	0.60	1.40	12.00
Sandstone	12	6	30.86	1.54	3.60	36.00

2.5. Test Methods

In the initial simulation phase, the working face underwent a standard excavation with a model working-face width of 80 cm (equivalent to 160 m in reality), as depicted in Figure 2. The excavation was incrementally conducted using a stepwise approach. This commenced 85 cm (170 m) from the model's left side to minimize the boundary's impact on the rock deformation. The excavation progressed sequentially to the right. Each simulated excavation step was 8 mm (equivalent to 1.6 m in reality). Continuous digital photography was employed to capture and observe the collapse and fracture developments of various rock layers. Following the completion of the coal-seam excavation, the criterion for stable subsidence was set at a maximum surface subsidence of 0.15 mm every 15 days (equivalent to 30 mm of subsidence over 6 months in reality). This indicated stabilized rock movement. The first phase was considered to be complete when this stability criterion was attained at the goaf surface, thereby transforming the model into a stable goaf area.

The second phase of the study simulated the flooding of the mine by groundwater. Water was injected into the voids of the mined-out area to mimic groundwater infiltration. Transparent glass plates were installed at the front and back of the area prior to the injection

to prevent rock fragments from falling. Following the injection, daily data collection was carried out and soil pressure measurements were obtained. The area was maintained in a saturated state for one week to ensure that the final settlement reached stability.

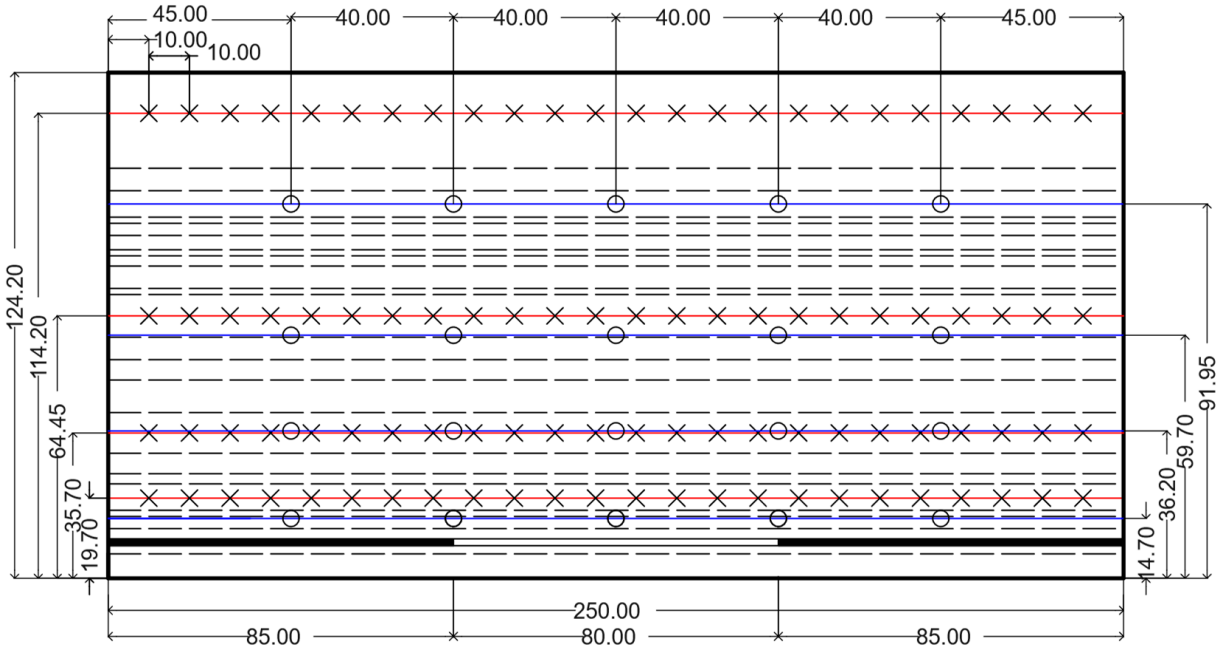

Figure 2. Arrangement of the measuring points of the model (cm). ○ denotes the pressure measurement point, × denotes the displacement measurement point.

3. Analysis

The overlying rock and the surface above the coal seam underwent certain deformations from the stage of coal-seam mining to the stage of rock stratum movement and stability. The deformation began in the rock stratum above the goaf. Successive caving, fracture, stratification, and bending then occurred, which spread to the surface. Subsidence basins within a certain range formed on the surface, and obvious caving zones, fracture zones, and bending zones appeared. The surface also gradually approached the final moving deformation value. Based on the stable state of overlying strata in the goaf, water was poured into the goaf to simulate a goaf affected by groundwater, and a secondary activation simulation analysis was conducted. The experimental results clearly revealed a significant displacement in the collapse zone.

3.1. Overlying Strata in Goaf Are Deformed after Water Filling Is Stabilized

The overlying rock was obviously damaged following the groundwater intrusion. The fractured rock layer had obvious subsidence compression, the rock blocks on both sides had gyration and slide instability, the fracture zone had obvious subsidence deformation, and the range of the fracture zone expanded upward. The deformation of the fracture zone above the goaf gradually stabilized after the water filling stabilized. The fracture zone developed upward and the bending zone as a whole deformed downward, as demonstrated in Figure 3.

3.2. Damage Mechanism Analysis of Overlying Rock in Goaf under Groundwater Action

With the closure of a mine, pumping and drainage cease and groundwater gradually accumulates. These closed coal mines cause the occurrence of water in the gob. After the ground surface movement and deformation in the goaf of a coal mine reach a basically stable state, the site may revert to being an unstable site under the action of underground water (this primarily refers to mine water). The instability of a site may be further intensified under the action of the above factors.

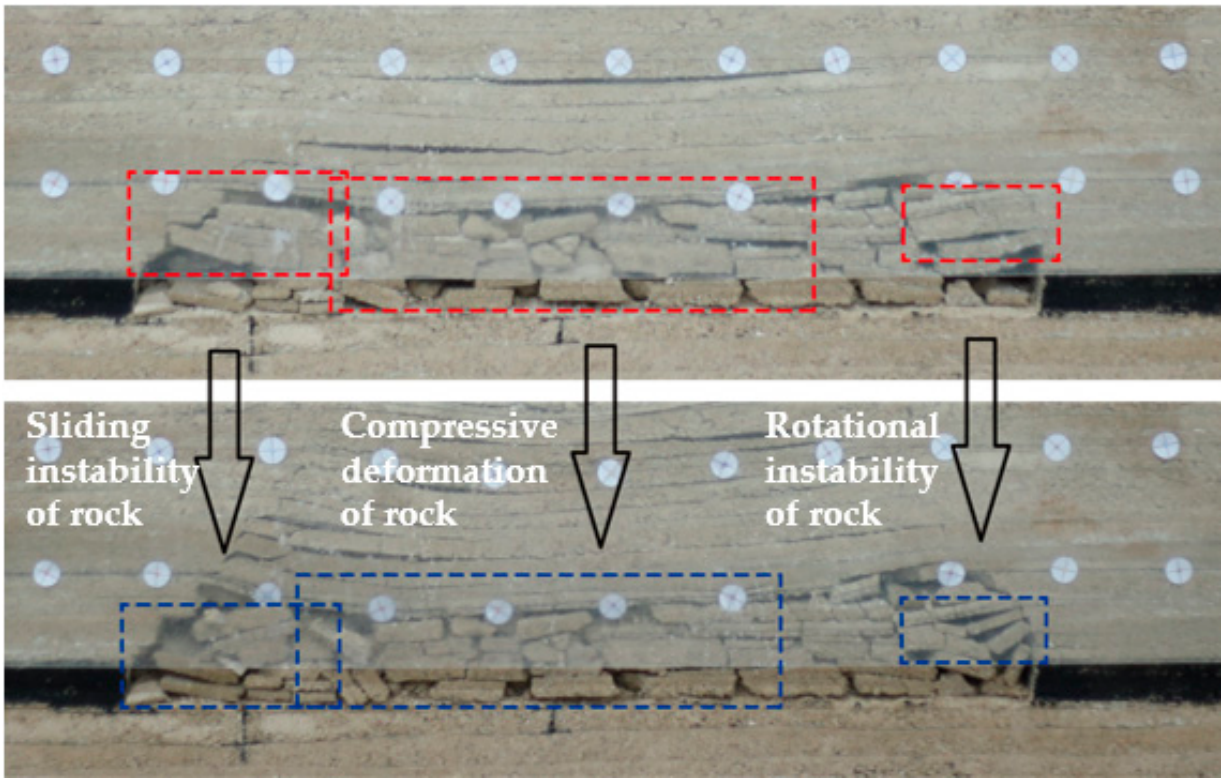

Figure 3. Comparison of overlying rock failure morphology before and after water filling.

The rock formation in the goaf was seriously damaged, and it was extremely easy to destroy the original environment of the groundwater so that the groundwater had an impact on the rock formation. The interaction between the groundwater and the rock mass (especially the rock mass in the goaf that had been damaged) as well as the stability of the rock formation were extremely vulnerable. The water on the discontinuous surface of the rock mass lubricated and reduced its friction resistance. This was reflected in the mechanics, which reduced the internal friction angle and intensified the shear movement of the rock mass. The water content of the rock mass increased, and the rock mass gradually became saturated after groundwater intruded into the gob. A weakening effect from a solid state to a plastic state occurred, potentially resulting in an argillation phenomenon. The softening effect reduced the mechanical properties, cohesion, and internal friction angle of the rock mass.

The groundwater had an obvious influence on the strength of the rock mass, and the intrusion of groundwater changed the physical state of the rock mass. The mechanical properties of the rock in a water-saturated state were obviously different from those in a dry state. The strength of the rock significantly decreased after it was soaked in water and gradually stabilized. As a result, the original stable state above the goaf was activated into an unstable state, or the unstable state was aggravated.

4. Discussion

The rock mass in a goaf is deformed under the influence of underground mine water. These changes are categorized into three types based on the various forms of deformation exhibited by a rock mass. These are compression deformation, rock block sliding instability, and rock block rotation instability. Each of these situations is explained below, and the main factors influencing their changes are analyzed.

4.1. Formation Mechanism of Caving-Zone Compression

The Mohr–Coulomb failure criterion is as follows:

$$\tau = \mathrm{C} + \sigma \mathrm{ntan}\varphi, \tag{3}$$

where τ is the shear strength, σ is normal stress, C is cohesion, and φ is the internal friction angle. The mechanical properties of a rock mass are reduced because of the softening and clayification of water, as are the cohesion and friction angles and the shear strength of the rock. Crushing occurs, and rocks with a small particle size are produced. These fill the voids, compact the pores and cracks, compress the caving zone, and increase the subsidence value of the overburden rock, as illustrated in Figure 4.

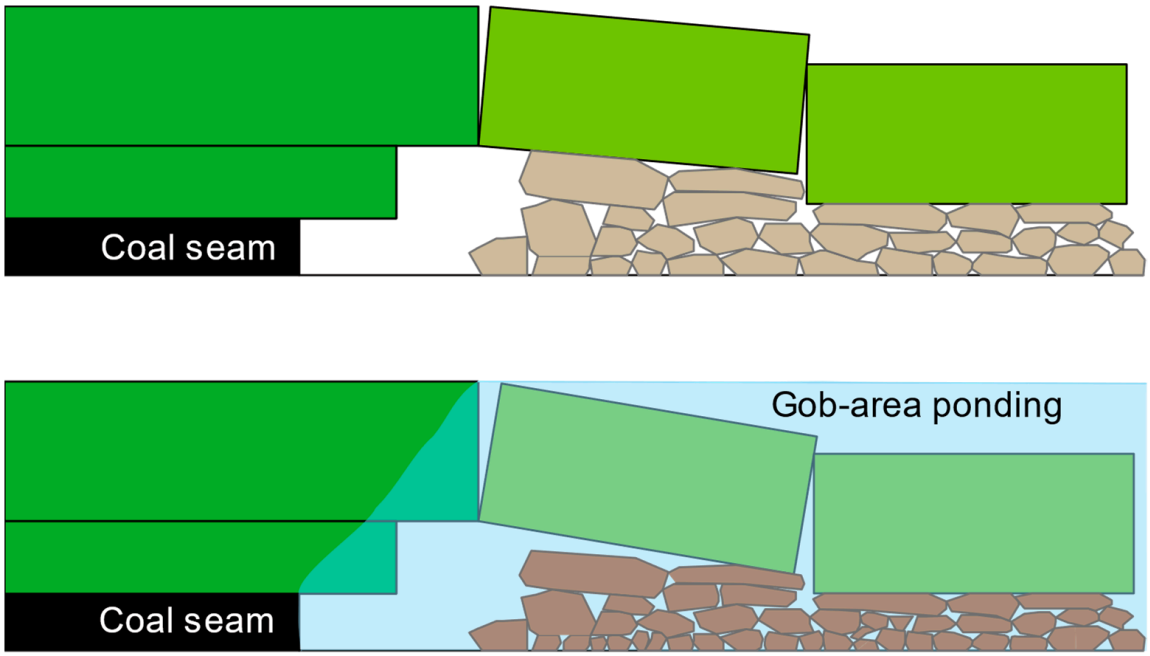

Figure 4. Formation mechanism of caving-zone compression.

Before groundwater intruded into the goaf in our study, key blocks sank. Key block B completely collapsed onto the crushed coal rock in the goaf, and the rotation of key block A was constrained by key block B at point B. Based on the assumption that the crushed rock below key block B was in a basic state of compaction, the subsidence of key block B was ascertained as follows:

$$W_1 = m - \sum h(K_p - 1). \tag{4}$$

After groundwater intruded into the goaf, the key block sank. A large number of studies [19–22] have demonstrated that the compression of a rock mass in a water-containing state is greater than in a dry state and that the compaction of a rock mass is caused by the action of groundwater, thus increasing W_1. An assigned coefficient (C) represents the ratio of the rock-filling water pressure to the original height. The subsidence amount of the key block under the influence of groundwater was calculated as follows:

$$\Delta W_1 = C \sum h(K_p - 1). \tag{5}$$

The comprehensive subsidence of the key blocks affected by groundwater was then

$$W_2 = m - C \sum h(K_p - 1), \tag{6}$$

where m is the mining height (unit m), K_p is the crushing expansion coefficient of the broken rock in the goaf, $\sum h$ is the unit m of the direct roof thickness, and $C < 1$.

4.2. Formation Mechanism of Rock-Slide Instability

The overlying strata moved to the goaf after the coal seam became stable. The stratum above the mined coal seam was broken, the broken rock blocks filled the goaf, and the broken rock blocks squeezed each other to form a three-hinged arch-balanced structure. The rock blocks were affected by the thrust of the left rock formation, the thrust of the right rock formation, and the supporting force of the underlying rock formation before mining. A mechanical equilibrium was maintained under the combined action of these forces. The balance depended on whether the extrusion pressure at the occlusal point exceeded the strength limit at the contact surface of the occlusal point. If it did, the instability caused the rock to slide back; if the friction force at the occlusal point was less than the shear force, the slide instability caused the roof step to sink.

The mechanical properties and the friction angle of the rock mass were reduced when local groundwater affected the rock mass in the goaf. It was then easy for the rock mass to slip and become unstable, even if the friction force at the occluded point was less than the shear force, as illustrated in Figure 5.

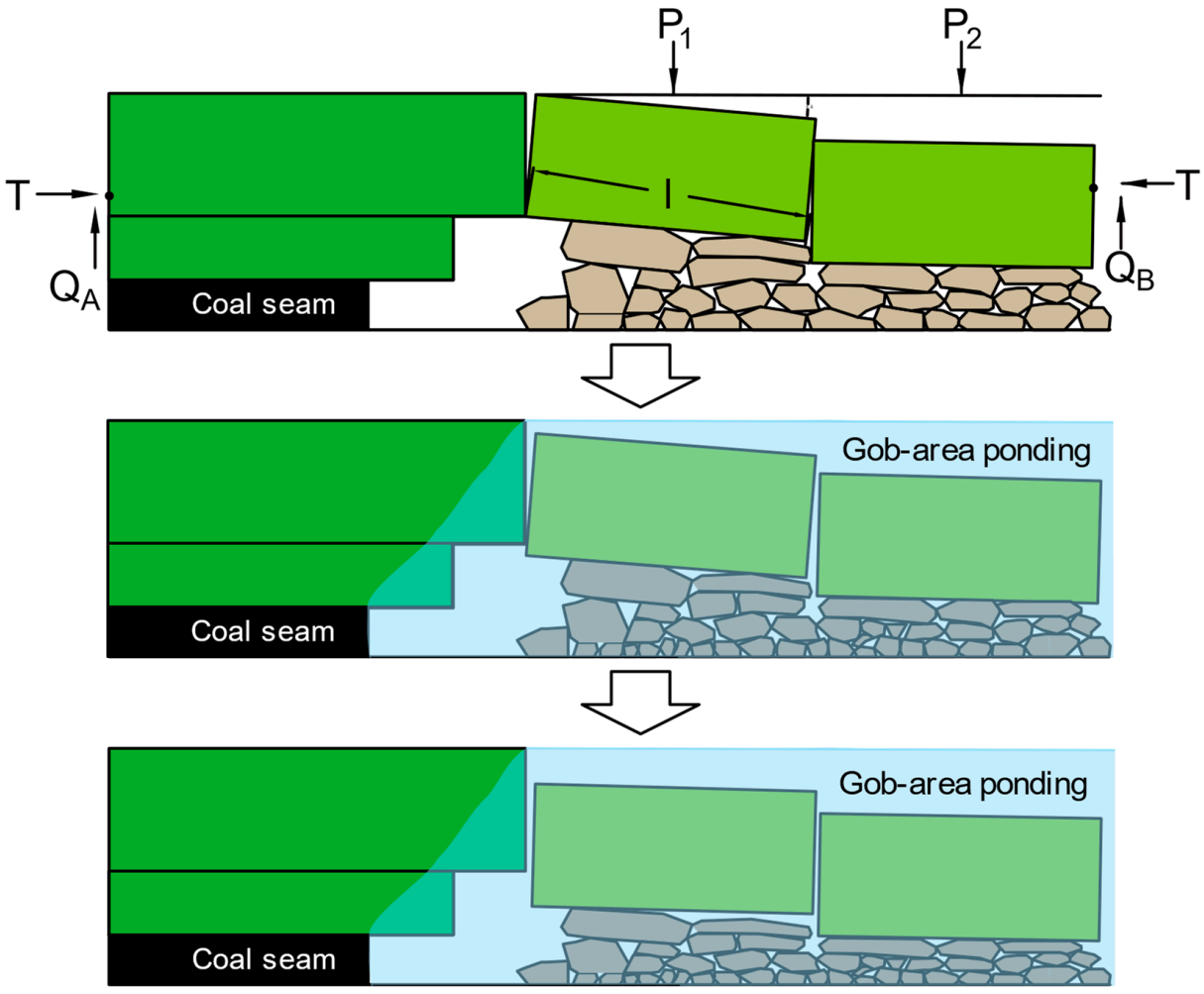

Figure 5. Formation mechanism of rock-slide instability.

According to Yan's research [23], rock strata migrate in the form of platform rock beams under shallow mining conditions. The stability of the stepped rock beam mainly depends on the relationship between the friction force and the shear force at the overlapping point of the rock blocks. If the shear force is greater than the friction force, the stepped rock beam structure slips and loses stability.

We used $i = h/l$ to denote the degree of fracture, which was $P_1 = Q_A + Q_B$. From the equilibrium equations $\sum MA = 0$ and $\sum MB = 0$, we derived the following equations:

$$T = \frac{P_1}{i - \sin\theta_1 + 2\sin\theta_2}, \tag{7}$$

$$Q_B = \frac{\sin\theta_1}{2(2i - \sin\theta_1)} P_1, \tag{8}$$

$$\theta_2 \approx \theta_1/4, \tag{9}$$

$$T = \frac{P_1}{i - \frac{1}{2}\sin\theta_1} \tag{10}$$

The maximum shear force Q_A of this structure occurred at point A. To prevent the structure from slipping and destabilizing at point A, the following condition had to be met:

$$T\ \mathrm{tg}\varphi \geqslant Q_A, \tag{11}$$

where $\mathrm{tg}(\cdot)$ and φ are the friction coefficients between rock blocks.

Substituting equations (6) and (8) into the above equation, we obtained the following:

$$tg\varphi \geqslant i - \frac{3}{4}\, sin\theta_1 \tag{12}$$

The degrees of the block and rotation angles were satisfied because the rock stratum was in a stable state before the action of the groundwater.

$$i \geqslant \mathrm{tg}\varphi + \frac{3}{4}\sin\theta_1 \text{ and } \theta_1 \leqslant \arcsin\left[\frac{4}{3}(i - \mathrm{tg}\varphi)\right], \tag{13}$$

The friction coefficient between the rock blocks decreased because of the action of the groundwater. The tan φ decreased, resulting in constant block and rotation angle degrees, as follows:

$$tg\varphi \leqslant i - \frac{3}{4} sin\theta_1, \tag{14}$$

Thus, the rock mass slipped and became unstable.

According to the research of Hou and Zhang [24–26] and our measured data, the value range of the degree of block i of the key block was $0.5 \leq i \leq 1.3$, and the value range of the rotation angle θ_1 was $0° \leq \theta_1 \leq 15°$, as demonstrated in Figure 6.

The smaller the rotation angle, the larger the degree of the block, the smaller the friction coefficient required to maintain stability, and the lesser the likelihood is of the rock mass sliding and becoming unstable under the influence of groundwater. The rock mass softens and is easy to fracture and break with the influence of groundwater intrusion. This results in a smaller block size and a decreased friction coefficient, which causes a rock mass to easily slip and become unstable.

When

$$i = h/l, \tag{15}$$

then

$$h + h_1 \geqslant \frac{\sigma_c}{30\rho g}\left(\mathrm{tg}\varphi + \frac{3}{4}\sin\theta_1\right)^2. \tag{16}$$

Therefore,

$$\mathrm{tg}\varphi \leqslant \sqrt{\frac{30\rho g(h + h_1)}{\sigma_c}} - \frac{3}{4}\sin\theta_1. \tag{17}$$

Whether stability is maintained is related to the bearing thickness of the structure $(h + h_1)$, and θ_1. σ_c gradually decreases with the action of groundwater; this aggravates the slide and instability of a rock mass. As the compressive strength decreases, an inequality is

more likely to be satisfied. This results in instability. The larger the $(h + h_1)$ and the smaller the θ_1, the greater the likelihood of instability, as demonstrated in Figure 7.

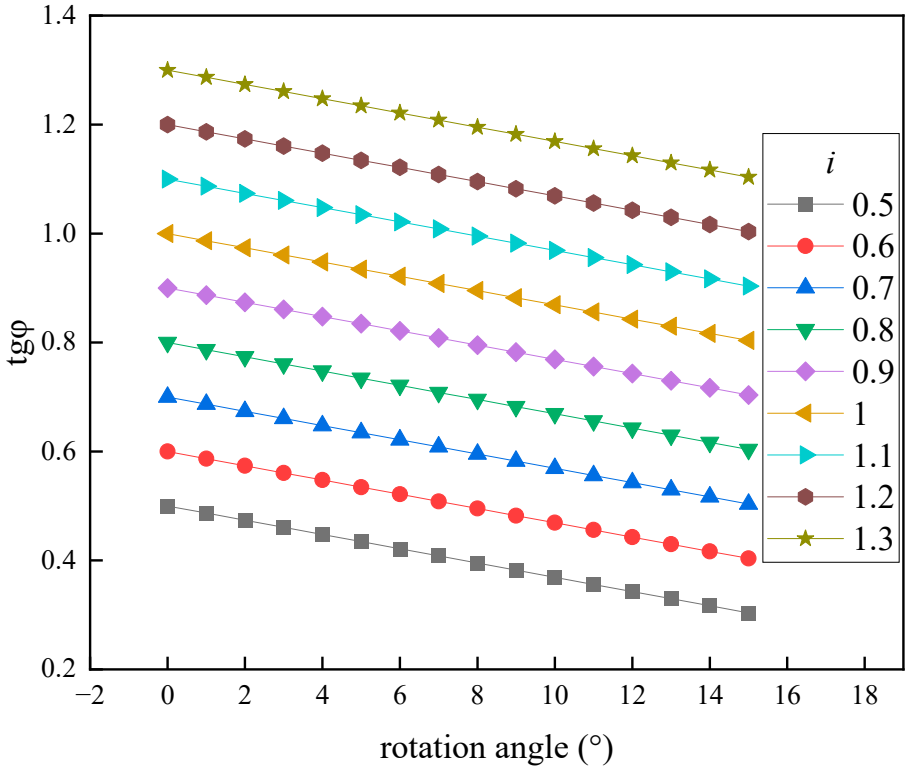

Figure 6. Relationship between θ_1 and friction coefficient under different i conditions.

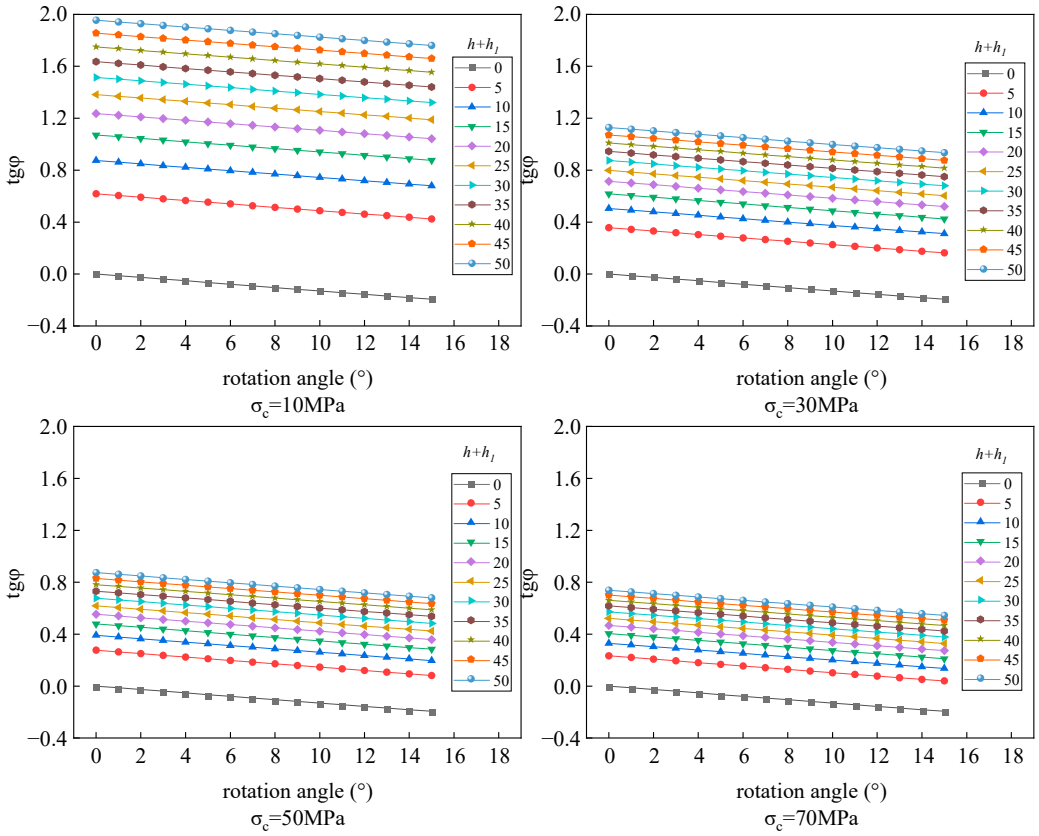

Figure 7. Relationship between $h + h_1$, θ_1, and friction coefficient under different σ_c conditions.

4.3. Formation Mechanism of Rock Rotation Instability

The third scenario involves the rotational instability of rock blocks, as illustrated in Figure 8.

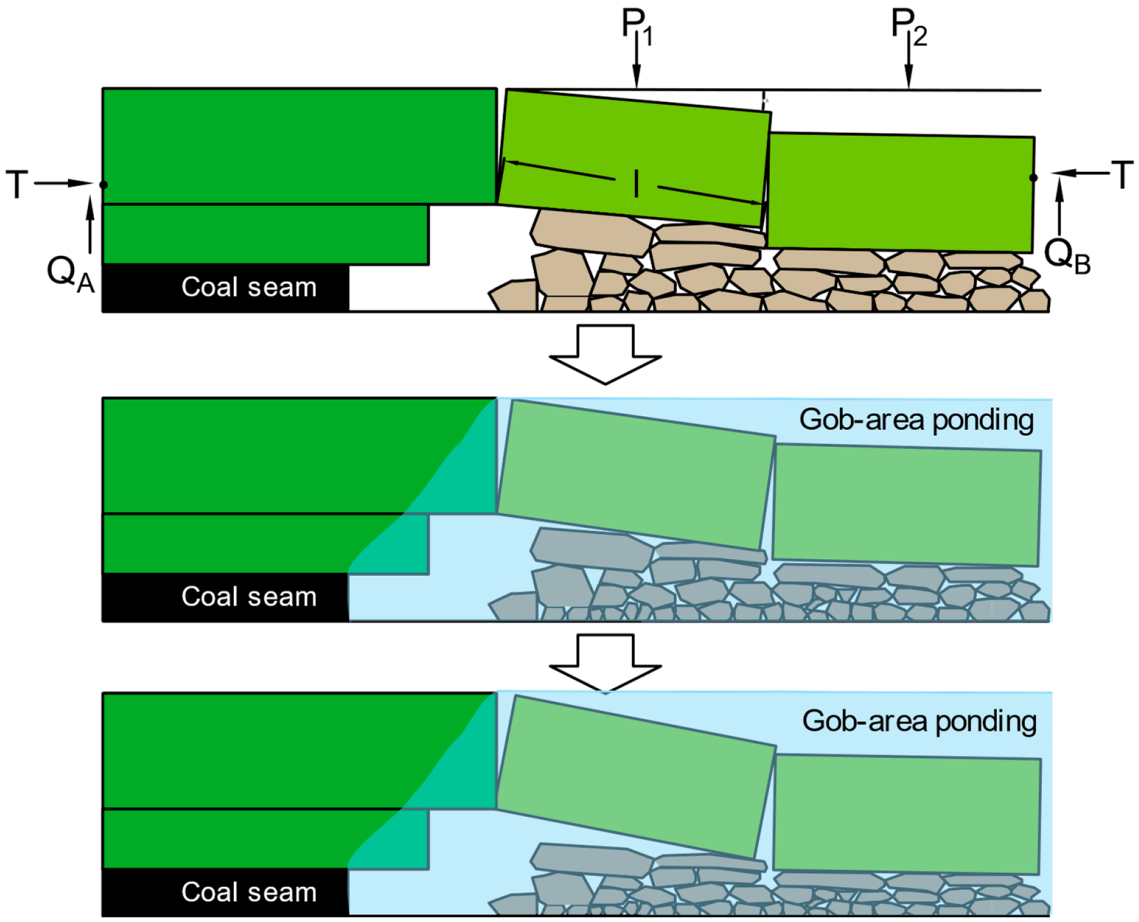

Figure 8. Formation mechanism of rotational instability.

The condition for preventing a rock mass from rotational deformation and instability is

$$T/\alpha \leqslant \eta\sigma_c, \tag{18}$$

where T/α represents the average extrusion stress on the contact surface and $\eta\sigma_c$ is the compressive strength of the block at the corner end. In view of the special condition of the corner (according to a large number of head tests), η = 0.3 is preferable. The relevant data can be obtained by substituting (16), as follows:

$$\sigma_c \geqslant \frac{20\rho g(h+h_1)}{3\left(i-\frac{1}{2}\sin\theta_1\right)(i-\sin\theta_1)}. \tag{19}$$

As the strength of the rock blocks decreases under the action of groundwater—that is, the compressive strength of the bearing layer, σ_c—the originally stable rock layer does not satisfy the above condition. This results in its rotational deformation and instability, as follows:

$$\sigma_c \leqslant \frac{20\rho g(h+h_1)}{3\left(i-\frac{1}{2}\sin\theta_1\right)(i-\sin\theta_1)}, \tag{20}$$

and

$$\sigma_c \leqslant \frac{20\rho g(h+h_1)}{3\left(i^2-\frac{3}{2}i\sin\theta_1+\frac{1}{2}\sin^2\theta_1\right)}. \quad (21)$$

The value of i has the most significant influence on the rotational instability of a rock mass. The greater the value of i, the greater the likelihood of rotational instability. When the value of i is constant, the values of $h+h_1$ and θ_1 are greater and it is more likely that rotational instability will occur, as demonstrated in Figure 9.

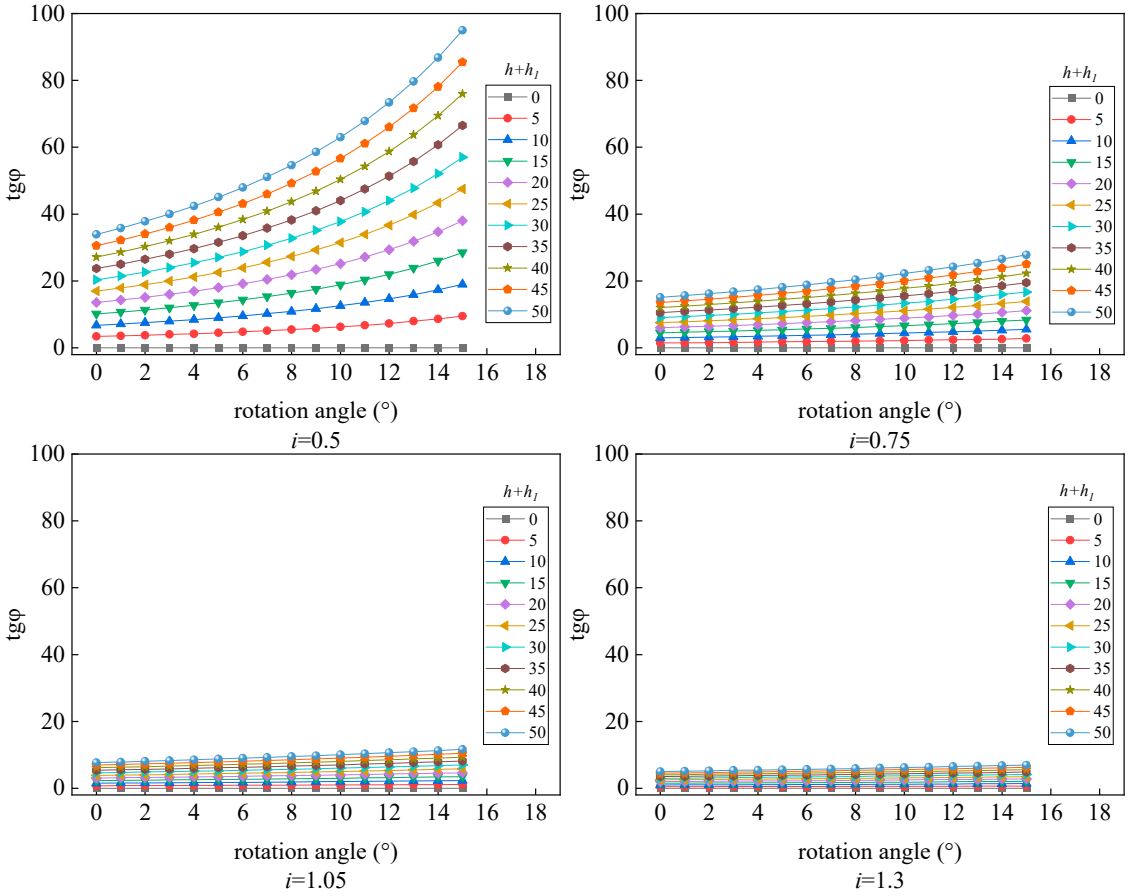

Figure 9. Relationship between $h+h_1$, θ_1, and friction coefficient under different i conditions.

5. Conclusions

It is important to understand the formation mechanisms of the failures and instability of overlying strata in a goaf under the action of groundwater for disaster prevention and environmental protection. In this study, we combined similar-material simulation tests and relevant working-face geological conditions with the "R–S" stability criterion under the influence of multiple factors (such as the block degree, internal friction angle, and rotation angle of key blocks) under the influence of groundwater to systematically analyze the failure and instability mechanisms of overlying rock in the goaf. Our summarized conclusions are as follows:

(1) Mine water affects the rock mass in mined-out areas. This leads to the activation of these zones, resulting in their deformation.

(2) Groundwater causes secondary damage to the overlying strata of a goaf, resulting in subsidence. This is mainly because of the softening and clayification of the rock mass by the water, which reduces the mechanical properties of the rock mass (such as the compressive strength of the bearing layer σ_c and the internal friction angle θ_1).

(3) The overlying rock in a goaf is affected by groundwater, and key blocks in the overlying rock exhibit sliding and turning instability. The stability of the overlying rock is related to the bearing thickness $(h + h_1)$, rotation angle (θ_1), and block degree (i).

(4) According to a stress analysis of the key blocks, the larger the $(h + h_1)$, the larger the i, and the smaller the θ_1, the greater the likelihood of rock block sliding and instability. The larger the i, $(h + h_1)$, and θ_1, the greater the likelihood of rock rotation instability.

(5) Compared with rock slide or instability deformation, generally speaking, the larger the i and $(h + h_1)$, the greater the likelihood of instability. The size of θ_1 determines whether rock slide instability or rotation instability occurs.

Author Contributions: Conceptualization, N.Z.; methodology, N.Z.; software, F.L; validation, D.S.; formal analysis, F.L.; investigation, D.S.; resources, F.L.; data curation, N.Z.; writing—original draft preparation, N.Z.; writing—review and editing, F.L.; visualization, F.L.; supervision, N.Z.; project administration, N.Z.; funding acquisition, N.Z. All authors have read and agreed to the published version of the manuscript.

Funding: This research was funded by the Scientific Research Projects of Universities in Anhui, grant number 2023AH052244; the Doctoral Research Initiation Fund, grant number 2022BSK007; and a School-Level Key Scientific Research Project, grant number 2023yzd05.

Data Availability Statement: The data are provided in this paper.

Conflicts of Interest: The authors declare no conflicts of interest.

References

1. Bell, F.G.; Stacey, T.R.; Genske, D.D. Mining subsidence and its effect on the environment: Some differing examples. *Environ. Geol.* **2000**, *40*, 135–152. [CrossRef]
2. Kim, K.-D.; Lee, S.; Oh, H.-J.; Choi, J.-K.; Won, J.-S. Assessment of ground subsidence hazard near an abandoned underground coal mine using GIS. *Environ. Geol.* **2006**, *50*, 1183–1191. [CrossRef]
3. Chen, S.; Zhang, L.; Jiang, N.; Yin, D.; Gao, Z.; Guo, W. A case of large buildings construction above old mine goaf in Shandong Province. *J. China Coal Soc.* **2022**, *47*, 1017–1030.
4. Liu, H.; Zhu, X.; Cheng, Y.; Su, L.; Dai, L.; Zheng, L.; Fang, S.; Jiang, M.; Zhang, Q.; Sun, Q.; et al. Key technology of human environment and ecological reconstruction in high submersible level coal mining subsidence area: A case study from Lvjin lake, Huaibei. *J. China Coal Soc.* **2021**, *46*, 4021–4032.
5. Wu, Z.Y. Geological Disaster Models in the Mined-out Subsidence Area in the Mountainous Areas of Northern Hebei and Their Hazard Mechanisms. Ph.D. Thesis, China University of Mining and Technology, Xuzhou, China, June 2021.
6. Gui, H.; Hu, R.; Zhao, H.; Li, J.; Song, X.; Wang, M.; Yu, H.; Fang, H. Overview of surface water hazards in China coalmines. *Water Pract. Technol.* **2019**, *14*, 851–862. [CrossRef]
7. Majdi, A.; Hassani, F.P.; Nasiri, M.Y. Prediction of the height of destressed zone above the mined panel roof in longwall coal mining. *Int. J. Coal Geol.* **2012**, *98*, 62–72. [CrossRef]
8. Cigna, F.; Tapete, D.; Lee, K. Geological hazards in the UNESCO World Heritage sites of the UK: From the global to the local scale perspective. *Earth-Sci. Rev.* **2018**, *176*, 166–194. [CrossRef]
9. Zhou, Y.W.; Zhang, T.; Duan, L.C. Summary of research on comprehensive treatment of mine goaf mine goaf in China. *Saf. Environ. Eng.* **2022**, *29*, 220–230.
10. Zhu, C.; Pang, S.H.; Zhao, J.Z.; Tao, Z.; Han, W.; Yin, X. Analysis of slope deformation caused by subsidence of goaf on tonglushan ancient minerelics. *Geotech. Geol. Eng.* **2019**, *37*, 2861–2871.
11. Cui, X.M.; Gao, Y.G.; Yuan, D.B. Erratum to: Sudden surface collapse disasters caused by shallow partial mining in Datong coalfield, China. *Nat. Hazards* **2014**, *74*, 911–929. [CrossRef]
12. Shi, H.; Zhang, Y.B.; Tang, L. Physical test of fracture development in the overburden strata above the goaf and diffusion process of permeable grout slurry. *Bull. Eng. Geol. Environ.* **2021**, *80*, 4791–4802. [CrossRef]
13. He, R.; Han, Z.; Liu, Y. Sensitivity analysis of stability factors of goaf based on numerical simulation orthogonal test. *China Min. Mag.* **2022**, *31*, 109–117.
14. Yadav, A.; Behera, B.; Sahoo, S.K.; Singh, G.S.P.; Sharma, S.K. An approach for numerical modeling of gob compaction process in longwall mining. *Min. Metall. Explor.* **2020**, *37*, 631–649. [CrossRef]
15. Salmi, E.F.; Karakus, M.; Nazem, M. Assessing the effects of rock mass gradual deterioration on the long-term stability of abandoned mine workings and the mechanisms of post-mining subsidence—A case study of Castle Fields mine. *Tunn. Undergr. Space Technol.* **2019**, *88*, 169–185. [CrossRef]
16. Xiao, Z.M.; Pae, K.D. The interaction between a penny-shaped crack and a spherical inhomogeneity in an infinite solid under uniaxial tension. *Acta Mech.* **1991**, *90*, 91–104. [CrossRef]

17. Luo, F.; Yang, B.S.; Hao, B.B.; Sun, L.; Fu, M. Mechanical properties of similar material under uniaxial compression and the strength error sources. *J. Min. Saf. Eng.* **2013**, *30*, 93–99.
18. Yang, X.; Su, L.D.; Zhou, B.; Liu, Z.; Zhou, C. Experiment study on similarity ratio of similar material for model test on red-bed soft rock. *Rock Soil Mech.* **2016**, *37*, 2231–2237.
19. Qiu, J.J. Experimental study on mechanical properties of sandstones underdry and saturated conditions. *China Energy Environ. Prot.* **2017**, *39*, 35–40.
20. Ma, Z.G.; Guo, G.L.; Chen, R.H.; Mao, X.B. An Experimental Study on the Compaction of Water-Saturated Over-Broken Rock. *Chin. J. Rock Mech. Eng.* **2005**, *24*, 1139–1144.
21. Chen, X.X.; Su, C.D.; Tang, X.; Guo, W. Experimental Study of Effect of Water-Saturated State on Compaction Property of Crushed Stone from Coal Seam Roof. *Chin. J. Rock Mech. Eng.* **2014**, *33* (Suppl. S1), 3318–3326.
22. Yu, B.Y.; Chen, Z.Q.; Wu, J.Y.; Li, Q.; Ding, Q.L. Experimental Study of Compaction and Fractal Properties of Grain Size Distribution of Saturated Crushed Mudstone with Different Gradations. *Rock Soil Mech.* **2016**, *37*, 1887–1894.
23. Yan, W.; Dai, H.; Chen, J. Surface crack and sand inrush disaster induced by high-strength mining: Example from the Shendong coal field, China. *Geosci. J.* **2018**, *22*, 347–357. [CrossRef]
24. Hou, Z.J. Analysis of combinatorial key strata stability in shallow coal seam with thick loose bed. *J. China Coal Soc.* **2000**, *25*, 127–131.
25. Hou, Z.J. Rotary end angle contact surface size of main roof fracture rock mass. *J. Min. Saf. Eng.* **1999**, *Z1*, 29–31.
26. Zhang, J.; Hou, Z.J.; Ma, L. Sand inrush in roof rock's rotating in shallow seam mining. *J. Xi'an Univ. Sci. Technol.* **2006**, *26*, 158–166.